V15

Characterization of silicon strip sensors

Theodor Zies
theodor.zies@tu-dortmund.de

Can Toraman
can.toraman@tu-dortmund.de

Measurements: 19.04.2024

Hand-in: 03.05.2024

TU Dortmund – Physics department

Contents

1 Objective

The objective of this experiment is to understand the workings of a silicone strip detector and its properties. Additionally, the use of readout electronics and resulting data is supposed to further introduce the participant into their usage in different detector systems.

2 Theory

In order to understand a silicone strip detector it is important to look at the theory of semiconductors.

2.1 Semiconductors

Semiconductors are defined by the energy gap between the valence and the conduction band. If the bands overlap in a material it is referred to as *conductor* since the electrons can move freely in the material. If the energy gap is to large the electrons can't travel into the conduction band, therefore these materials are called *insulators*. If though the energy gap is in the range below 3 eV the material is a *semiconductor*. The semiconductor employed in this experiment is silicone with a band gap of 1.107 eV [1]. Silicone has four valence electrons and arranges itself in a diamond lattice structure. When for example through thermal excitation or other external particles an electron leaves the valence band a hole is created. This hole behaves like to a quasi-particle, carrying a positive charge. The electron and the hole can form a bound state resembling an atom, if the material is placed into an electric field (e.g. by placing a cathode/anode to the material) the formation of such a state is prevented. The electrons and holes can now travel to the cathode/anode. This behavior can be modified by a process called *doping*, in which some of the silicone particles in the crystalline structure are replaced by elements that carry a higher/lower amount of valence electrons.

2.1.1 n-type semiconductor

If the element used for doting has a valence charge higher than four (e.g. Arsenic: five valence electrons), one electron is not used for the binding in the crystalline structure and can therefore move almost freely in the material.

2.1.2 p-type semiconductor

Analog to the n-type semiconductor, the introduced material has fewer electrons in its valence band (Boron: three valence electrons). The boron would then leave one of the bonds with the surrounding silicone atoms partially empty, creating a hole. A schematic representation of both doting methods is given in Figure 1.

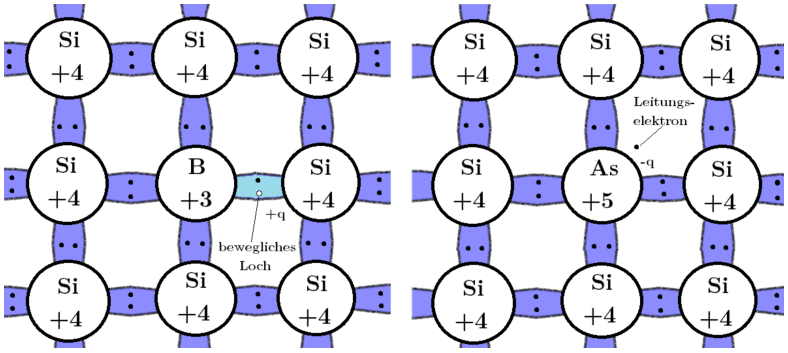

Figure 1: Graphical representation of boron and arsenic doping in silicone[1].

2.1.3 pn transition

If one connects a p- and n-doped material together a so-called diode is created. Inside the diode the additional electrons from the n-side now tend to recombine with the holes from the p-side. This results in a positive charge on the n-side and a negative on the p-side. The resulting difference of a few mV is called diffusion voltage U_{D} [1].

For the detection of ionizing particles a voltage is applied to either side of the diode, the electrons coming from the applied potential recombine with the holes on the p-side and the electron in the n-side flow into the anode, resulting in a zone in which no free charge carriers remain. This zone is called the *depletion zone* and its dimension can be determined to be

$$d(U) = \sqrt{\frac{2\epsilon(U_{\mathrm{D}} + U)}{eN_{\mathrm{eff}}}}, \tag{1}$$

where U is the voltage applied to the diode, ϵ the dielectric constant of silicone, e the elementary charge and N_{eff} the effective charge carrier density. N_{eff} is determined by

$$N_{\mathrm{eff}} = \frac{N_{\mathrm{D}} N_{\mathrm{A}}}{N_{\mathrm{D}} + N_{\mathrm{A}}},$$

where N_{D},N_{A} are the respective densities of the n and p doped materials. When the depletion zone is as large as the diode itself, one speaks of a full depletion at the depletion voltage U_{dep}. Using the fact that the applied voltage usually is smaller than the depletion voltage, the formula for the depletion voltage can be determined as follows:

$$U_{\mathrm{dep}} \approx \frac{e}{2\epsilon} N_{\mathrm{eff}} D^2$$

Where D is the the thickness of the diode. If the applied voltage is below the depletion voltage then the distance $d_{\mathrm{c}}(U)$ can be approximated with

$$d_{\mathrm{c}}(U) = D\sqrt{\frac{U}{U_{\mathrm{depl}}}}.$$

Ideally, the diode is fully depleted so the signal generated by an ionizing particle can be detected. Through thermal effects electrons can still enter the current band and create the so called *leakage current*. This effect increases with higher voltages. The relation between the current and the voltage can be seen in Figure 2.

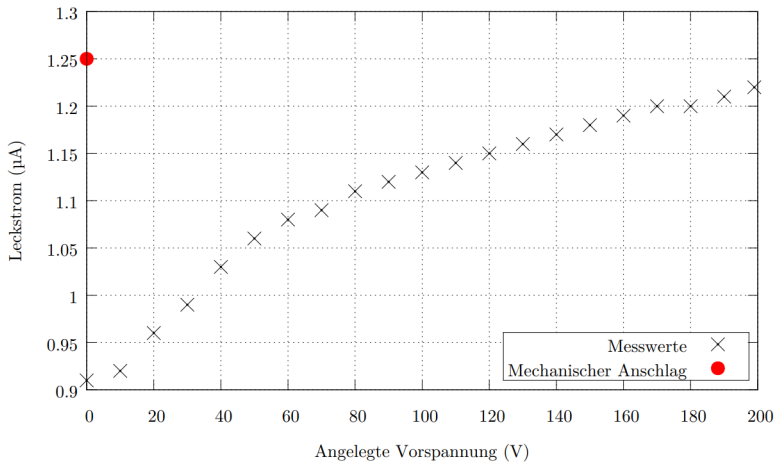

Figure 2: Current measured across the sensor in relation to the applied voltage [1].

By using this plot, the depletion voltage can be determined as the voltage at which the leakage current only increases linearly.

2.2 Ionizing radiation

The silicone strip detector can be used to detect ionizing particles. During the experiment a source producing beta particles is employed.

2.2.1 Beta decay

The used source is the strontium isotope ^{90}Sr, which decays via a β^- decay into yttrium (maximal energy 0.545 MeV), that later decays into zirconium (maximal energy 2.28 MeV) [1].

$$^{90}\mathrm{Sr} \rightarrow {}^{90}\mathrm{Y} \rightarrow {}^{90}\mathrm{Zr}$$

During a β^- decay a neutron in the atomic nucleus decays into a proton, an electron and an anti-electron-neutrino. Since this process is a three body decay the electron is not produced at a fixed energy. The energy of the emitted electron follows the distribution shown in Figure 3

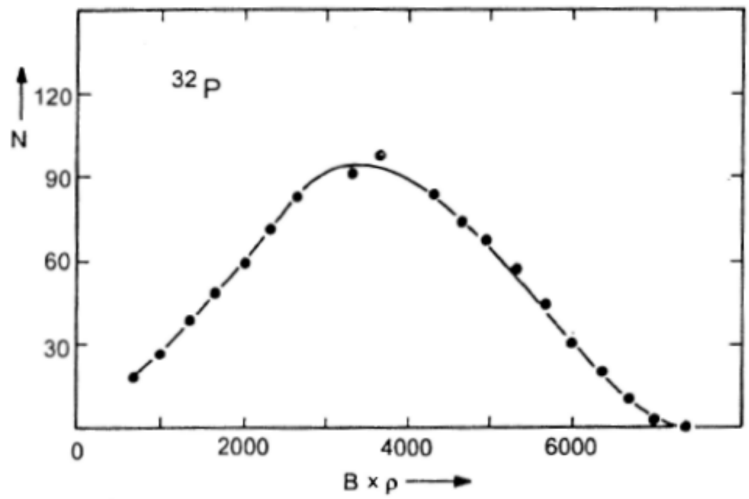

Figure 3: Energy distribution of a electron originating from an β^- decay [1].

The activity is defined as the rate of change of the number of nuclei $A = -\dot{N}$. From this it can be deduced that the activity can be written as

$$A = \lambda N_0 \exp(-\lambda t) = A_0 \exp(-\lambda t),$$

where A_0 and N_0 are the activity and number of nuclei at $t = 0$, and λ is the decay constant of the decaying material/particle.

2.2.2 Interaction in matter

Due to the relatively low energy of the electrons, their energy loss is predominantly caused by collisions with the nuclei of the material they traverse. The ionizing particles inside the detector are detected by these collisions, as they excite the electrons in the crystalline structure of the detector material. These exited electron then create a measurable signature in the detector. The energy deposited by the electrons can be determined using the Bethe-Bloch equation with additional correction terms:

$$-\frac{\mathrm{dE}}{\mathrm{d}x} = 2\pi N_\mathrm{a} m_e c \rho \frac{Z}{A} \frac{1}{\beta^2} \left[ln\left(\frac{\tau(\tau+2)}{2(I/m_e c^2)^2} \right) + F(\tau) - \delta - 2\frac{C}{Z} \right],$$

with

$$F(\tau) = 1 - \beta^2 + \frac{\frac{\tau^2}{8} - (2r_e + 1)\ln(2)}{(\tau+1)^2}, \qquad \text{where } \tau = \gamma - 1.$$

The meaning of the symbols and their values can be seen in [1]. From this formula it can be determined that the electron originating from the ^{90}Sr source is depositing 3.88 MeV per cm [1].

Usually for particles traversing a silicone detector the deposited energy can be approximated by a Gaussian distribution. As for a thinner detector (e.g. like the 300 µm of the detector used in this experiment) the thickness is not sufficient enough for the energy loss to be described as Gaussian. The actual distribution is much better described by a Landau distribution. Another effect at play stems from the already described energy distribution of the emitted electron. This results in a convoluted Landau distribution, as shown in Figure 4.

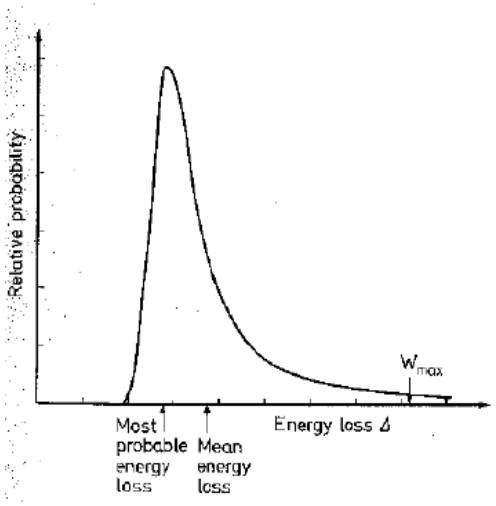

Figure 4: Convoluted Landau distribution, describing the energy loss of particle inside a thin material [1].

2.3 Noise and pedestals

Most electronics and detectors will create noise which interferes with the intended measurement. So the recorded counts from the Analog-Digital-Converter (ADC) can be described by

$$\mathrm{ADC}(i,k) = \mathrm{P}(i) + \mathrm{D}(k) + \mathrm{Signal}(i,k),$$

ADC is the probability of the detection a signal k at the i-th strip on the detector. $\mathrm{P}(i)$ is the so called *pedestal*. It is determined as the mean value of the $\mathrm{ADC}(i,k)$ without $\mathrm{Signal}(i,k)$. So $\mathrm{P}(i)$ is calculated for N measurements as

$$\mathrm{P}(i) = \frac{1}{N}\sum_{k=1}^{N}\mathrm{ADC}(i,k). \tag{2}$$

The $\mathrm{D}(k)$ contribution is the *common mode shift* and is calculated using

$$\mathrm{D}(k) = \frac{1}{128}\sum_{i=1}^{128}(\mathrm{ADC}(i,k) - \mathrm{P}(i)) \tag{3}$$

From these distributions, the root mean square is used to determine the noise:

$$\text{Noise}(i) = \sqrt{\frac{1}{N-1}\sum_{k=1}^{N}(\text{ADC}(i,k) - \text{P}(i) - \text{D}(k))^2} \tag{4}$$

3 Experimental setup

The experimental setup consists of a control unit, the detector unit and a computer with an application for the visualization and data taking. The control unit is connected to the detector unit using a ribbon cable and to the computer via a USB connection. Located on the control and detector unit is a glass fiber connection that is used to point a laser from the control unit onto the detector. Additionally, a strontium-90 source is provided, along with the shielding for its application.

3.1 Detector unit

The detector unit mainly consists of the silicon strip detector with 128 strips and a BEETLE readout chip. The silicon strip detector consists of a n doped silicone base with inlayed p doped silicone strips. The strips are then isolated by a SiO_2 layer to which the readout electronics are connected. The thickness of the silicone strip sensor is 300 µm. A schematic diagram of the sensor is shown in Figure 5b and a macroscopic picturfe is given in Figure 5a [1].

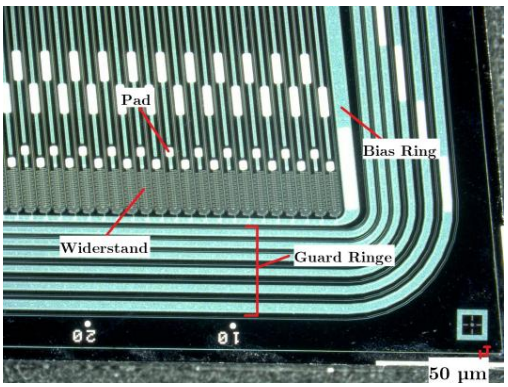

(a) Macroscopic picture of the silicone strip sensor [1].

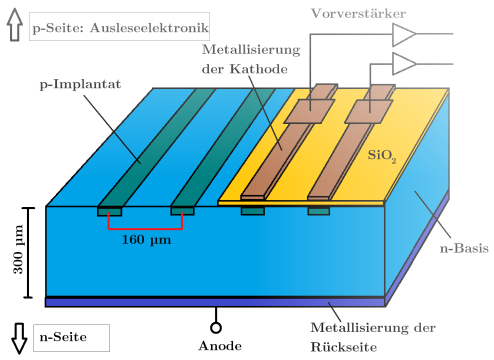

(b) Schematic diagram of the silicone strip sensor[1].

In the case of a not fully depleted sensor, some of the electrons and holes generated by the ionizing particles are recombined outside of the depletion zone. The charge collection efficiency (CCE) describing this process when applying a laser is given by

$$\text{CCE}(U) = \frac{1 - \exp\left(\frac{-d_c(U)}{a}\right)}{1 - \exp\left(\frac{-D}{a}\right)}, \tag{5}$$

where a is the penetration depth of the laser.

3.2 Laser

The Laser employed in this experiment is fed into the detector unit using an optic fiber cable. It has a wavelength of 980 nm, a diameter of 20 µm, a pulse length of 5 ns, and a peak power of 0.2 mW. The position and the focusing of the laser can be adjusted using two micrometer screws.

3.3 Control unit

The control unit houses the laser and is used to regulate the voltage applied to the silicone sensor. It can also measure the leakage current of the sensor. The data acquired by the control unit is transferred to the computer and can be collected there using the Alibava system.

4 Experimental procedures

Before starting the experiment, it is advisable to become familiar with the experimental setup and the software. In the initial measurement, the current passing through the sensor is recorded at intervals of 10 V for the applied voltages. This is performed until a voltage of 20 V above the expected depletion voltage is reached.

The first measurement using the software is performed in a *pedestal run* of 1 000 events, in order to determine the pedestal and the noise.

Before using the laser or the radioactive source, a set of calibration measurements are started. The first calibration is used to determine the optimal delay. It is started using the *Delay measurement* button in the Alibava software. After this run, five different channels are used in a *Calibration run*, with the applied voltage above the depletion voltage. Another run is started afterwards with the applied voltage turned down to 0 V.

After the calibration measurement, the laser is lead into the detector unit using the optic fiber cable. It is then focused and moved along the sensor until a maximally high peak is achieved in the Alibava software. Initially the optimal delay between the laser signal and the chip readout is determined using the *laser sync.* function. Then the structure of the sensor is probed by recording 1 000 events at 35 10 µm intervals. During the next measurements the CCE is determined by recording 1 000 events from 0 to 200 V in 10 V steps.

A similar approach is used when measuring the radioactive source, with the difference of recording 10 000 events per scan.

Finally a last scan using the radioactive source is performed and 1 000 000 events are recorded.

5 Analysis

The following analysis is split into five parts, each focusing on one of the measurements decribed in section 4.

5.1 Depletion voltage

The first part of the analysis is the measurement of the current-voltage characteristic of the silicon strip sensor. In Figure 6, the measured leakage current is displayed with the corresponding applied bias voltage. A flattening of the curve at 60 V is cleary visible, this corresponds exactly to the depletion voltage $U_{\text{dep}} = 60\,\text{V}$ of the chip stated by the manufacturer. For the following measurements, the bias voltage is set to 80 V to ensure the chip is always fully depleted.

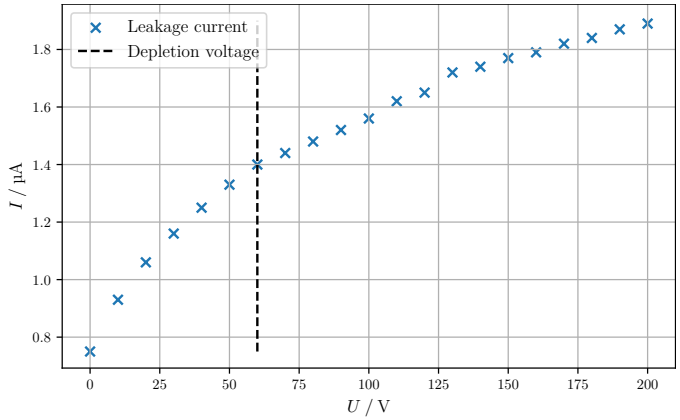

Figure 6: Plot of the measured current-voltage characteristic.

5.2 Pedestal run

The data collected during the pedestal run is evaluated to determine the noise of the strips. The pedestal for each strip is calculated by taking the mean value of the ADC counts of all events for each individual strip, as given by (2). The common mode shift for each event is then aquired by substracting the pedestal from the ADC counts of each strip and again taking the mean value according to (3). At last, the noise is determined by plugging the previous results into (4). A bar diagram of the pedestals and noise is shown in Figure 7.

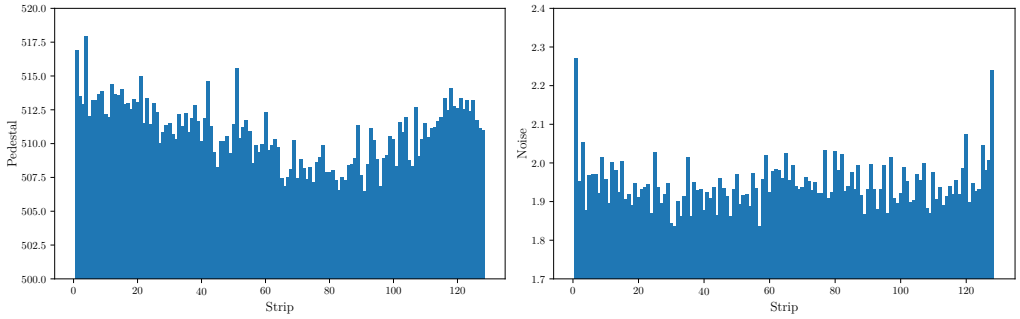

(a) **(b)**

Figure 7: Bar diagrams of the pedestals (a) and noise (b) of the 128 individual strips.

The diagrams show a visible increase of the pedestals and noise towards the edges of the chip, this might have something to with the structure of the chip or the way the signal is read out. A histogram of the common mode shift is displayed in Figure 8.

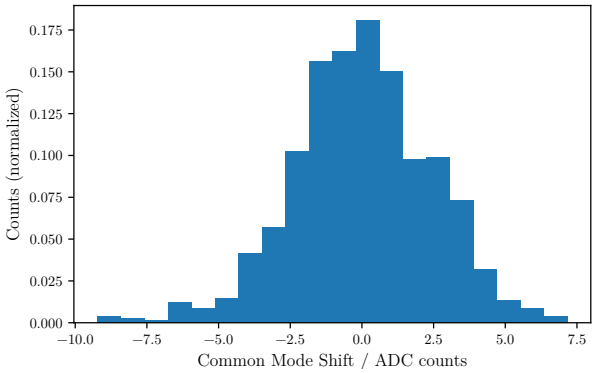

Figure 8: Commong mode shift measured during the pedestal run.

As expected, the common mode shift also referred to as *common noise* follows a gaussian distribution centered around 0.

5.3 Calibration measurements

In this section, the data aquired from the calibration run is analysed. The results from the delay measurement are shown in Figure 9.

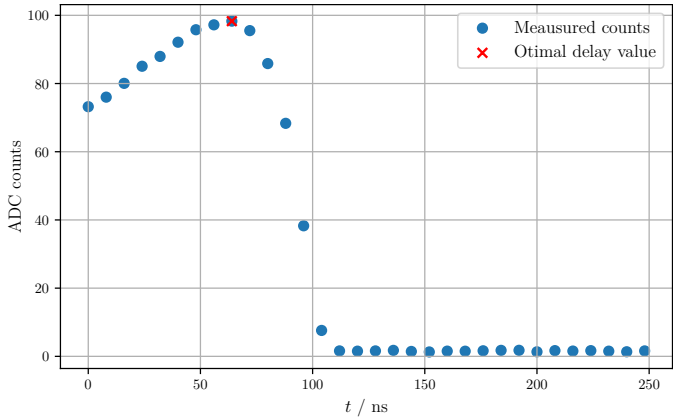

Figure 9: Results from the delay measurement.

Figure 9 shows the ADC counts depending on the delay of the chip readout. The highest counts were archieved at 64 ns, which is why this value was set as the delay for the rest of the experiment. After this, a calibration curve is measured for five different channels. This curve shows the relation between the injected charge and the ADC counts. The five curves are given in Figure 10a. As one can see in Figure 10b, an additional curve at 0 V is recorded for channel 60 and compared to the regular curve of this channel.

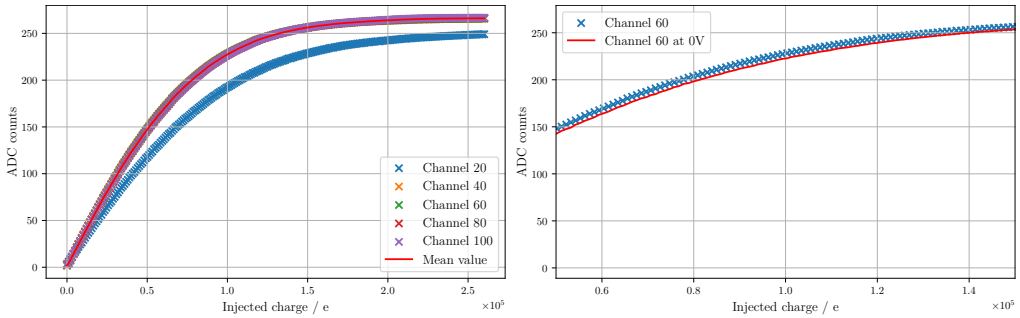

(a) **(b)**

Figure 10: Calibration curve of five channels (a) and detailed view of channel 60 at 0 V (b).

As seen in Figure 10a, all channels show almost exactly the same calibration curve. For some unknown reason, channel 20 meausured significantly less ADC counts. This is why it is excluded from the determination of the average value of all channels. For the next step, the mean value of the five channels is taken. The calibration curve at 0 V is slightly lower than the one measured above the depletion voltage. This behaviour is expected, as the depletion region is smaller if no bias voltage is applied. This directly leads to fewer charges being registered and thus lower ADC counts, as it can be seen in Figure 10b. To further quantify this dependecy of the counts from the injected charge, a 4-th degree polynomial is fitted to the mean counts of the five channels. The polynomial is of the

form

$$Q(\mathrm{ADC}) = a \cdot \mathrm{ADC}^4 + b \cdot \mathrm{ADC}^3 + c \cdot \mathrm{ADC}^2 + d \cdot \mathrm{ADC} + e\,. \tag{6}$$

The result of the fit is shown in Figure 11. Here, the fit range is restricted to values below 250 ADC counts to get a good result.

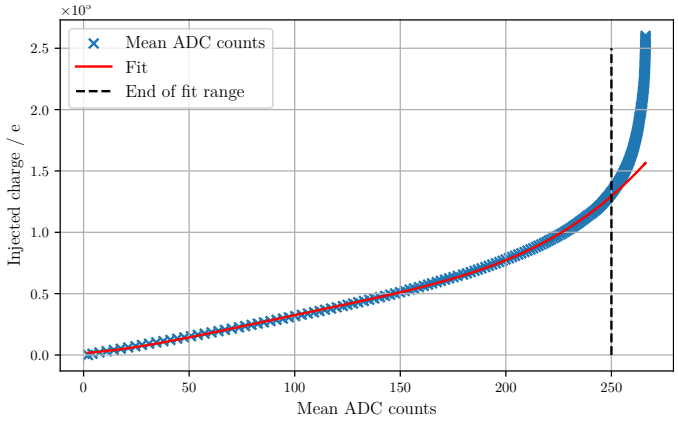

Figure 11: Fit of 4-th degree polynomial to the mean ADC counts of the calibration run.

The fit yields the following coefficients for (6)

$$\begin{aligned} a &= (7.7 \pm 0.4) \times 10^{-5}\,\mathrm{e} \\ b &= (-2.93 \pm 0.21) \times 10^{-2}\,\mathrm{e} \\ c &= (4.1 \pm 0.4)\,\mathrm{e} \\ d &= (115 \pm 24)\,\mathrm{e} \\ e &= (1.6 \pm 0.5) \times 10^{3}\,\mathrm{e}\,. \end{aligned}$$

These coefficients together with (6) now allow any ADC counts to be converted into an electric charge.

5.4 Measuring the strip sensor by using the laser

The physical structure of the sensor and its strips is determined by using the laser. Before the measurement can be started, the optimal delay between laser signal and chip readout is determined by plotting the data from the *Laser Sync* run. This is shown in Figure 12, where it is cleary visible that the maximal ADC counts are archieved at a delay of 100 ns.

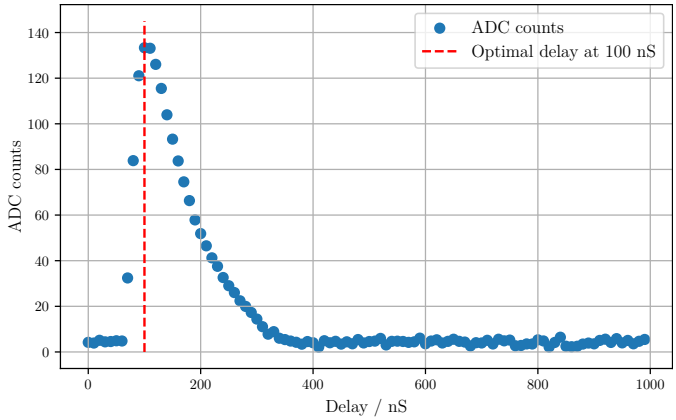

Figure 12: Results of the *Laser Sync* run.

After moving the laser across the 35 µm intervals, a heatmap is produced showing the signal of the relevant channels that were hit by the laser. Figure 13 shows the affected channels (82-85) and their signal strength depending on the laser position.

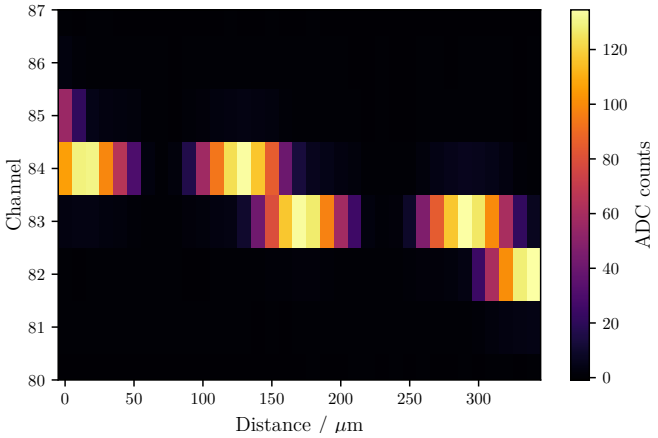

Figure 13: Heatmap of the signal strength of the affected channels depending on the laser position.

In the following, the individual signal for channel 83 is analysed in Figure 14. The position of the beginning, peak and end of the signal is also shown.

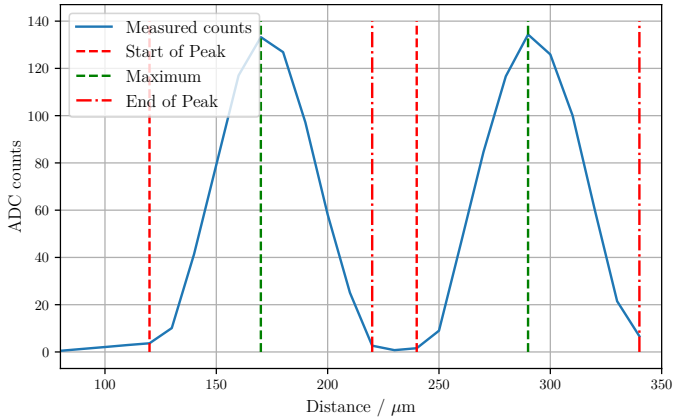

Figure 14: Signal strength of channel 83 depending on the laser position.

The width of the strip is simply the distance between the two peaks, as this is the position where the laser is on the channel but reflected by the metal of the strip. The extension of the laser can be estimated by the distance between the start of a peak and its maximum. All relevant positions are marked in Figure 14 and the resulting values are:

$$\begin{aligned} \text{width of strips} &= 290\,\mu\text{m} - 170\,\mu\text{m} = 120\,\mu\text{m} \\ \text{laser extension} &= 170\,\mu\text{m} - 120\,\mu\text{m} = 50\,\mu\text{m}\,. \end{aligned}$$

The distance of two strips can be determined by comparing the position of the maxima of two different channels in Figure 13:

$$\text{distance} = 40\,\mu\text{m}\,.$$

The pitch is then calculated as the sum of the distance between the strips and their width:

$$\text{pitch} = 120\,\mu\text{m} + 40\,\mu\text{m} = 160\,\mu\text{m}\,.$$

5.5 Determination of the charge collection efficiency

The charge collection efficiency of the laser is determined by measuring the relation between the collected charge (ADC counts) and the applied bias voltage.

5.5.1 Using the laser

When using the laser, at first the channel on which the laser is focused during the measurement is to be determined. By plotting a heatmap of the ADC counts for each channel, one can see that the laser was focused on channel 73, as shown in Figure 15.

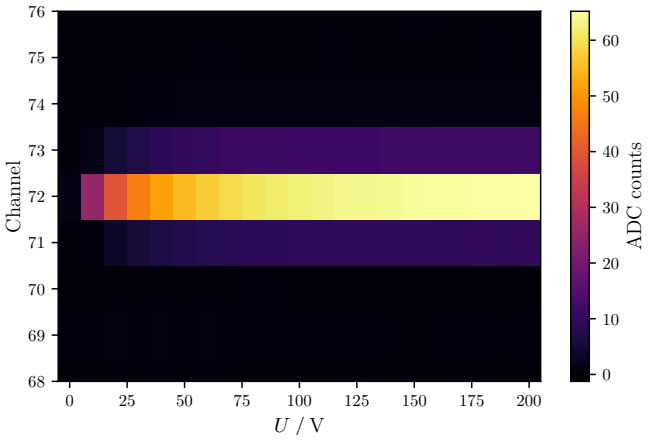

Figure 15: Heatmap showing the ADC counts of each channel and bias voltage.

Thus in the following, only the data from channel 73 are considered. In order to get the charge collection efficiency, the measured ADC counts have to be normalized in regard to the maximum ADC counts of the plateau. In theory, the plateau should show constant counts after the depletion voltage U_{dep} is reached, however the acutal data shows a slight increase in this area. This is why the counts are normalized in regard to the first value of the plateau, so that a proper fit of (5) can be performed. The normalized counts in dependence of the bias voltage are shown in Figure 16.

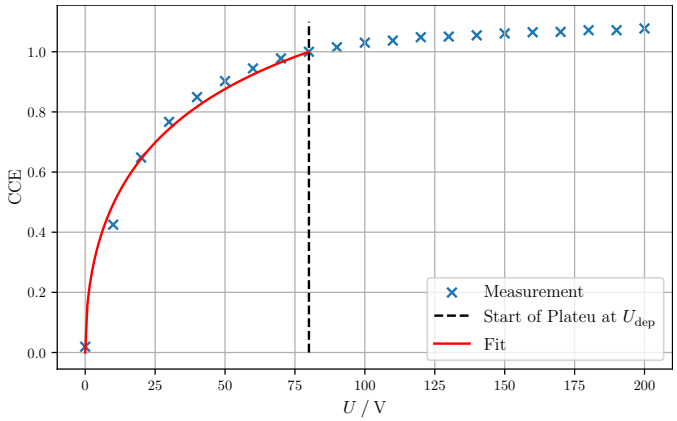

Figure 16: Charge collection efficiency of channel 73.

The fit was performed in the range $0\,\text{V} < U < 80\,\text{V}$. The depletion voltage of $U_{\text{dep}} = 80\,\text{V}$ is a fixed paramter in (5), whereas the value of the penetration depth a of the laser is determined via the fit as

$$a = (253 \pm 30)\,\mu\text{m}\,.$$

5.5.2 Using the beta source

The same curve is now measured by replacing the laser with a β^- radioactive source. The ADC counts are now determined in clusters. To get the charge collection efficiency, the entries in each cluster are first summed, then the mean value of all clusters is taken. A normalization is performed analogously to the one of the laser measurement. The resulting curve is displayed in Figure 17.

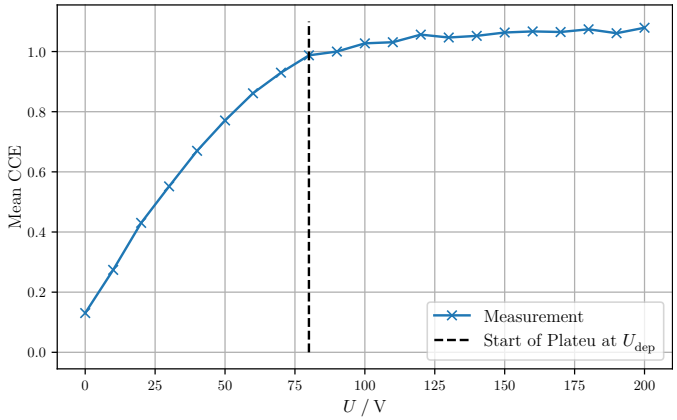

Figure 17: Charge collection efficiency determined via the β^- source.

A comparison of the measured curves with the two different methods is shown in Figure 18

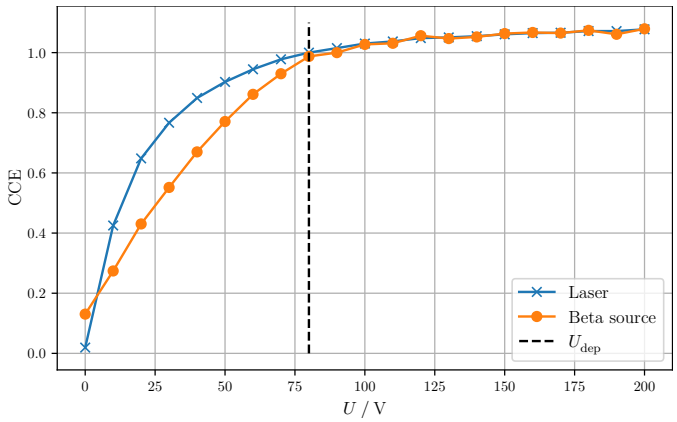

Figure 18: Comparison of the charge collection efficiency determined via the laser and the β^- source, respectively.

One can see that the curve measured using the laser increases earlier with the applied voltage. After reaching the depletion voltage, both curves fully agree again. This shows that the chip performs worse with detecting charged particles at lower voltages compared to just the photons emmited by the laser. If measurements are performed above the depletion voltage, this effect can be neglected as both methods yield the same charge collection efficiency there.

5.6 Large source scan

Finally, the large source scan containing roughly one million events is analysed. Figure 19 shows how the number of cluster per event is distributed as well as how many channels exist per cluster.

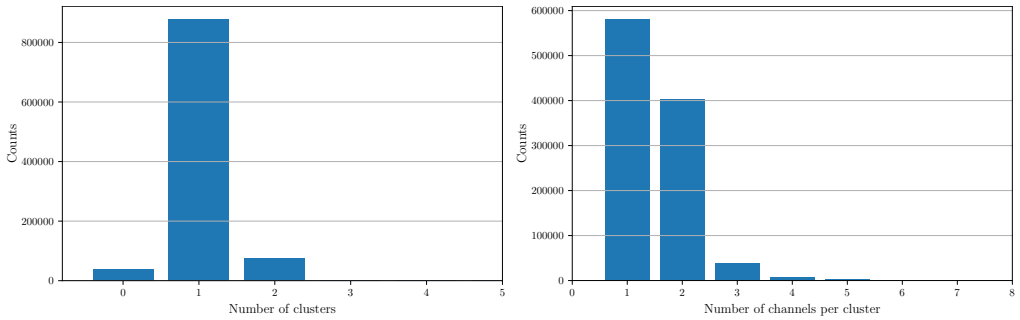

(a) **(b)**

Figure 19: Number of clusters per event (a) and number of channels per cluster (b).

One can see that an event mostly leads to the formation of one cluster, and each cluster usually contains the signal of one to three channels. Next, a hitmap is produced for all channels. This is displayed in Figure 20 and shows how many events/hits were registered by each individual channel.

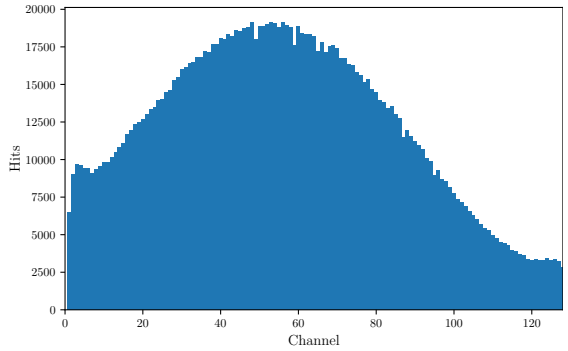

Figure 20: Hitmap displaying the events of each channel.

Most of the hits are registered in the middle of the chip, while the edges cleary show a lower amount of entries. Lastly, the distribution of the measured ADC counts as well as the energy spectrum is computed. To aquire the energy spectrum from the ADC counts, they are converted into electric pulses with the conversion formula (6) determined during the calibration run. The pulse is then converted into an energy by using the fact that the energy needed to generate an electron-hole pair is approximatly 3.6 eV [1]. Figure 21 shows both the aforementioned distributions.

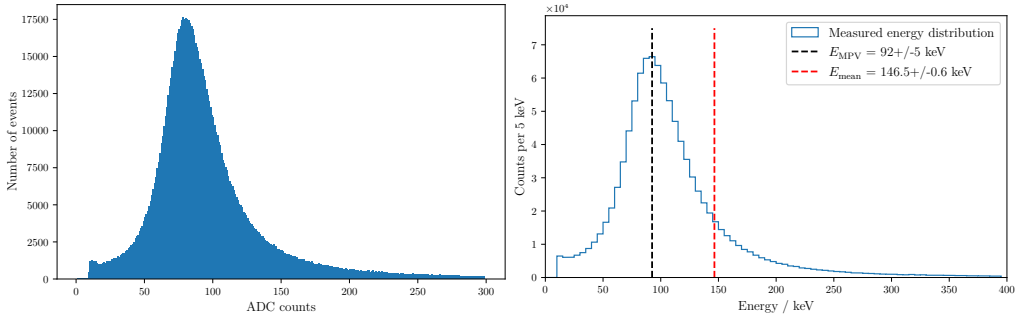

(a) **(b)**

Figure 21: Distribution of the ADC counts (a) and the energy (b).

The distribution of the energy spectrum allows to determine the most probable energy and mean energy of the β^- source:

$$E_{\text{MPV}} = (92 \pm 5)\,\text{keV}$$
$$E_{\text{Mean}} = (146.5 \pm 0.6)\,\text{keV}\,.$$

6 Discussion

6.1 Depletion voltage

In the first part, the depletion voltage is determined to be 60 V. Later, the depletion voltage is again measured by using the charge collection efficiency. In this case, a value of 80 V is obtained. The manufacturer [1] states a depletion voltage in the range of 60 to 80 V, so both measurements are acceptable. Both values are only estimations, as they are obtained by roughly determining the point where a curve flattens into a plateau. Therefore it is expected that they do not fully agree.

6.2 Measuring the strip sensors

The pitch of the strip sensors has been calculated from their measured width and distance to be 160 µm. This is the exact value given by the manufacturer [1], the high precision could be achieved through the 10 µm resolution chosen for the scan. The laser extension was measured at 50 µm and is thus significantly larger than the stated [1] 20 µm. This indicates that the laser was probably not fully focused during the measurement. A reason for this could be the fact that it was difficult to find an absolout maxima when adjusting the horizontal micrometer scew.
The charge collection efficiency curve shows a behaviour close to the theoretical one, with the exception that the plateau slighty increases for voltages above the depletion voltage. This might be a consequence of the noise, that increases with the bias voltage and is not fully removed from the data.

The value for the penetration depth $a = (253 \pm 30)\,\mu\text{m}$ seems consistent with the sensor thickness of $D = 300\,\mu\text{m}$ and the given pentration depths of lasers with slightly different wavelenghts in [1].

6.3 Energy spectrum

During the large source scan, the calculated energy spectrum resembles the expected convolution of a Landau and a Gauss distribution [1], where the most probable energy is lower than the mean energy. Using the modified Bethe-Bloch equation, it can be calculated that the average energy disposition of an ionising electron with the maximum energy of the primary ^{90}Sr decay in pure silicon is $3.88\,\text{MeV/cm}$. Multiplying this value by the sensor thickness D, the theoretically expected mean energy loss becomes $\bar{E}_{\text{theo}} = 116.4\,\text{keV}$. This can be compared to the measured mean energy loss

$$\begin{aligned} \bar{E}_{\text{theo}} &= 116.4\,\text{keV} \\ \bar{E}_{\text{exp}} &= (146.5 \pm 0.6)\,\text{keV}\,. \end{aligned}$$

A deviation of $20.5\,\%$ is observed, which is quite large. A possible reason might be an underestimation of the noise in the sensor, furthermore the modified Bethe-Bloch equation is only an approximation with limited precision.

References

[1] *V15-Characterization of silicon strip sensors.* TU Dortmund, Department of physics.